SUPPLEMENTARY FIGURES

Complement activation shapes immune contexture and immunotherapy response in clear cell renal cell carcinoma

Mikel Rezola Artero[1#*], Idris Boudhabhay[1,2,3#*], Margot Revel[1], Houcine Hamidi[1,4], Alaeddine Redissi[1], Nicolas S. Merle[1,3], Emma Fleury[1], Matt Siellet[1], Antonin Bourdin[1], Marina de Castro Deus[1], Jeanne Bouthenet[1], Isaias Hernandez-Verdin[1], Cheng Ming Sun[1], Guilhem Pupier[1], Antoine Bougouin[1], Rafael Sanchez-Salas[5], Petr Macek[5], Lara Rodriguez-Sanchez[5], Xavier Cathelineau[5,6], Adrián Ransom-Rodríguez[5,7], Virginie Verkarre[8,9] Sophie Siberil[1], Catherine Sautes-Fridman[1], Marie-Agnes Dragon-Durey[1,3,4], Yann A Vano[1,3], Stephane Marie Oudard[10], Wolf Herman Fridman[1] and Lubka T Roumenina[1,3,*]

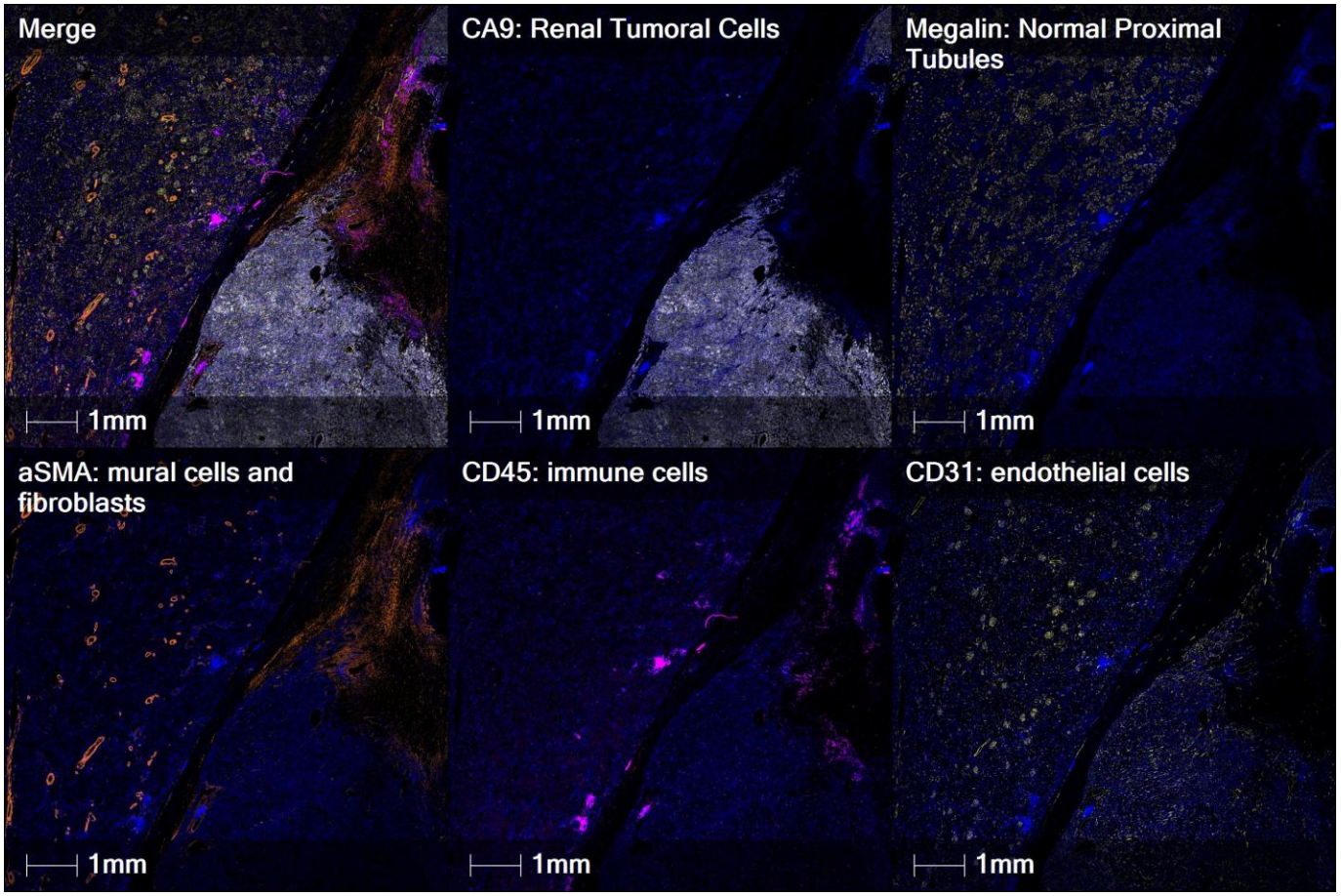

Fig. S1. Multiplex immunofluorescence panel for spatial profiling of the ccRCC microenvironment. Representative immunofluorescence images of a slide showing: CA9 (white) for ccRCC malignant cells in the tumor core, megalin (brown) for proximal tubular cell in the normal adjacent tissue, CD31 (yellow) for endothelial cells highlighting blood vessels, αSMA (cyan) for mural cells and fibroblasts and CD45 (purple) for immune cells infiltrating the tissue.

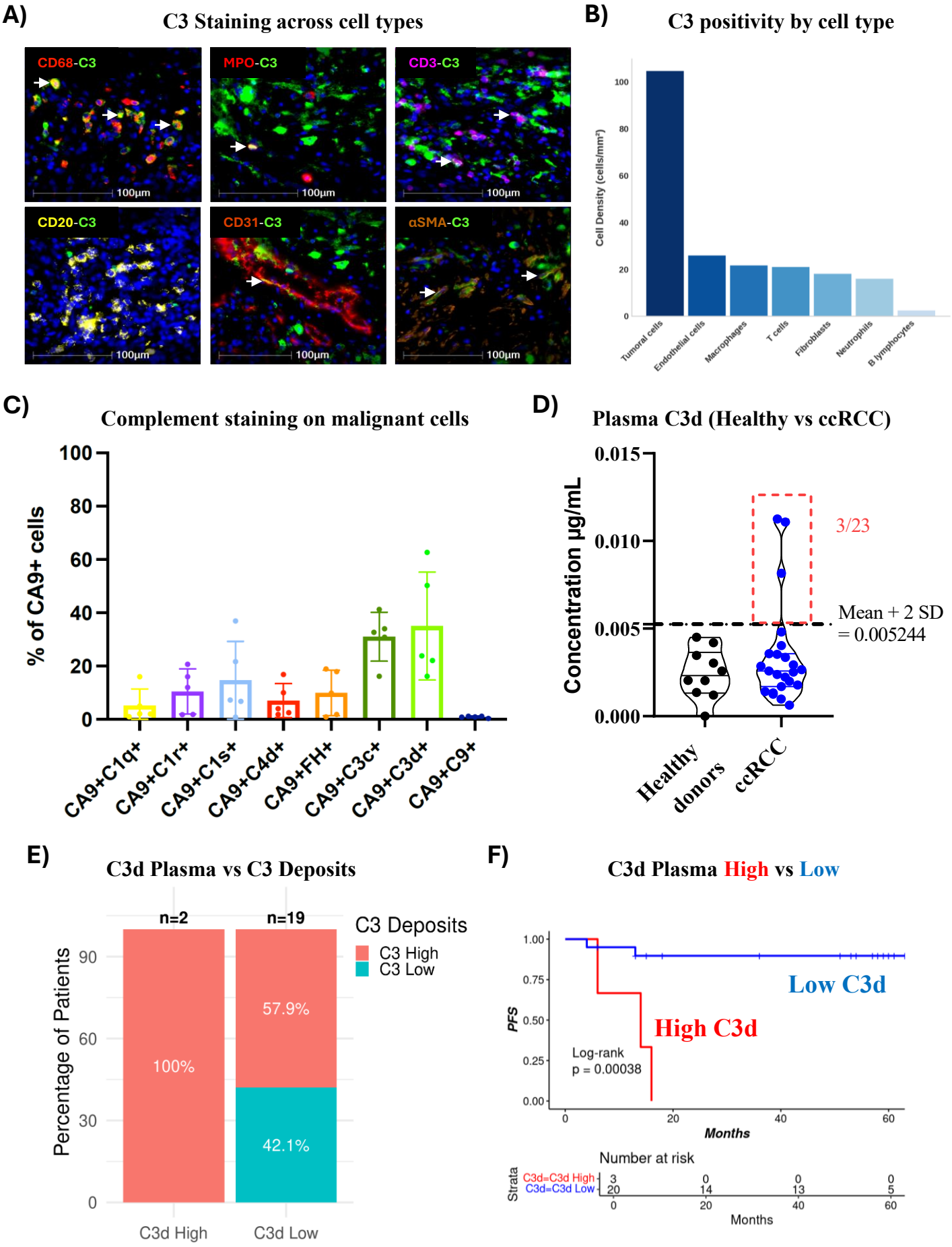

Fig. S2. ***In situ*** **complement profiling reveals dominant C3 deposition on tumor cells, with low systemic detection of C3d despite prognostic relevance.**

Fig. S2. In situ complement profiling reveals dominant C3 deposition on tumor cells, with low systemic detection of C3d despite prognostic relevance. (A) Identification of C3 positive cells in ccRCC highlighting colocalizations of C3 with CD68+ cells (macrophages), MPO+ cells (neutrophils), CD3+ cells (T cells), CD20+ cells (B cells), CD31+ (endothelial cells) and αSMA+ cells (mural cells and fibroblasts). **(B)** Density of C3 positive cells by cell type, evidencing high density of positivite malignant cells in ccRCC. **(C)** Frequency of complement marker positivity on malignant cells across 5 ccRCC primary tumors**. (D)** Comparison of plasma C3d levels between treatment-naïve ccRCC patients (n = 23) and healthy controls (n = 10) **(E)** Association between plasma C3d levels above normal range and high C3 deposits in the primary tumor. **(F)** PFS of ccRCC treatment-naïve patients (ExhauCRF) according to C3d circulating levels in plasma.

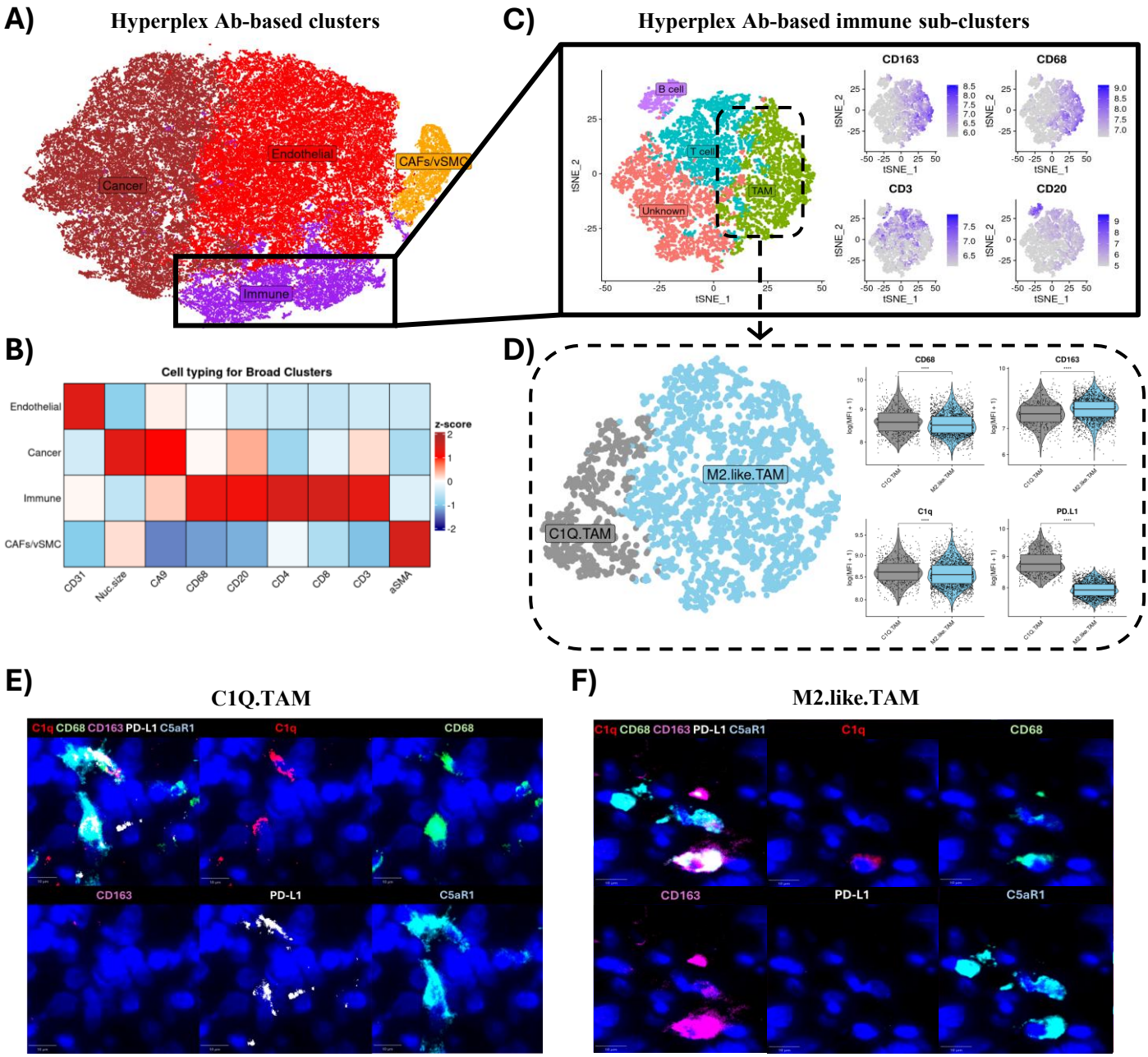

Fig. S3. Cell annotation of ccRCC tumor cells using hyperplex analysis validates TAM subclusters at protein level. (A) t-SNE projection showing unsupervised clustering of single cells from annotated ccRCC tumor cells, identifying endothelial cells, vascular smooth muscle cells and cancer-associated fibroblasts (CAFs/vSMC) and immune cells. **(B)** Heatmap of scaled mean marker positivity of segmented cell clusters validating cluster annotations. **(C)** Clustering results from the immune cell cluster (left), identifying B cells, T cells, TAMs and an uncharacterized subpopulation of immune cells ("unknown"); and marker expression across immune clusters (right). **(D)** Re-clustering results from the TAM cluster identifying the C1Q-TAM and M2-like-TAM subclusters (left); and marker positivity of key TAM markers (right). Representative immunofluorescence images showcasing **(E)** C1Q-TAMs, and **(F)** M2-like-TAMs; C1q: red; CD68: green; CD163: purple; PD-L1: white; C5aR1: cyan. Nuclei are stained with DAPI.

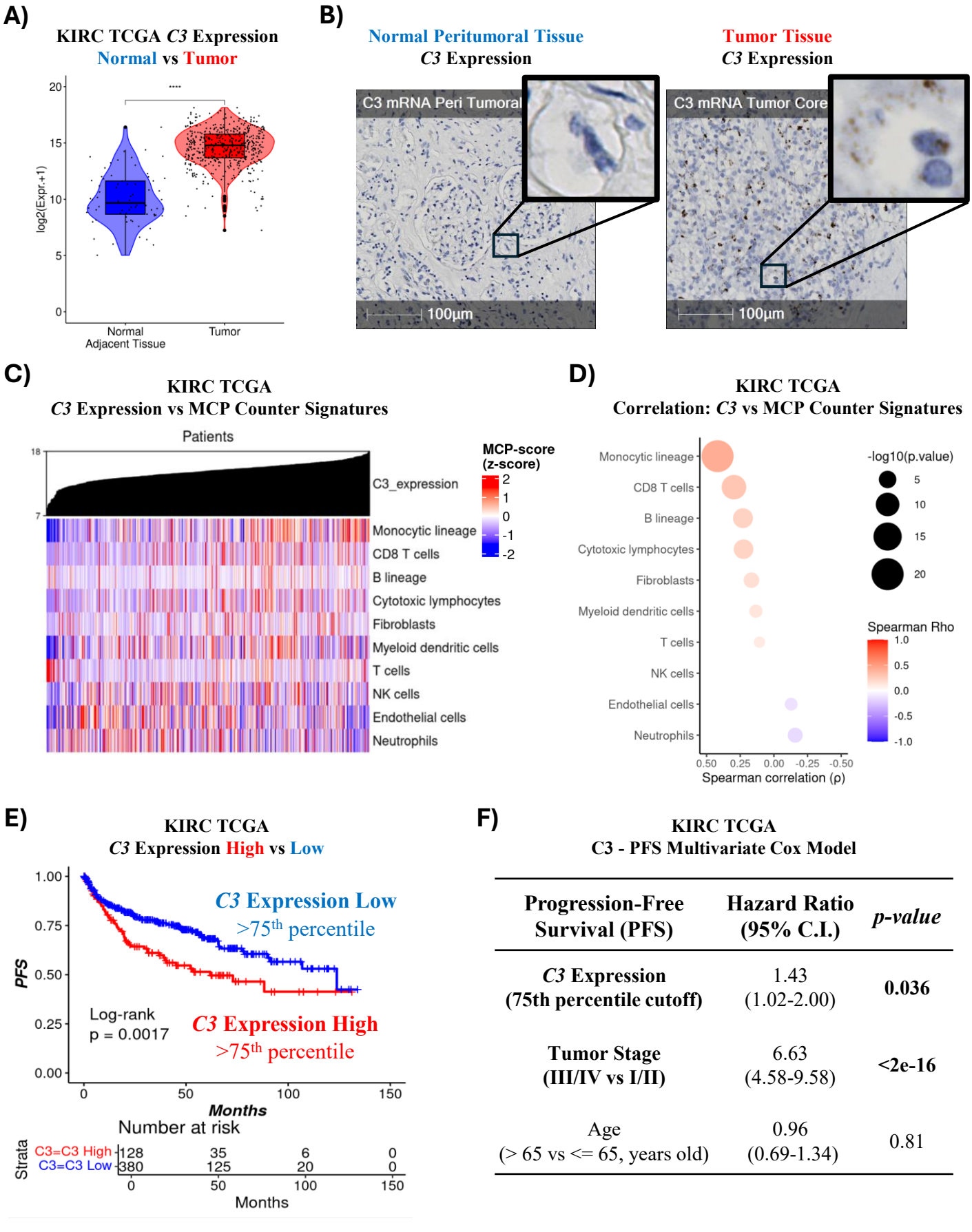

Progression-Free Survival (PFS)	Hazard Ratio (95% C.I.)	*p-value*
***C3* Expression (75th percentile cutoff)**	1.43 (1.02-2.00)	**0.036**
Tumor Stage (III/IV vs I/II)	6.63 (4.58-9.58)	**<2e-16**
Age (> 65 vs <= 65, years old)	0.96 (0.69-1.34)	0.81

Fig. S4. *C3* is overexpressed within ccRCC tumors and associated with increased myeloid infiltration and worse clinical outcomes in the TCGA-KIRC cohort.

Fig. S4. *C3* is overexpressed within ccRCC tumors and associated with increased myeloid infiltration and worse clinical outcomes in the TCGA-KIRC cohort. (A) *C3* expression in ccRCC tumors (n=510) vs healthy adjacent tissue (n=70) from the KIRC TCGA cohort. **(B)** *C3* gene expression assessed by RNAscope on normal peritumoral tissue (left) and tumor tissue (right). **(C)** Heatmap (MCPcounter signatures as rows x patients as columns) showing scaled MCPcounter signatures across patients ordered by *C3* expression (n=510). **(D)** Bubble plot evidencing the correlation between C3 expression and MCPcounter signatures across patients from the KIRC TCGA cohort (color scale denotes the correlation strength and bubble size corresponds to the statistical significance). **(E)** Progression-Free Survival Kaplan–Meier curves according to *C3* expression (upper quartile cut-off) in the KIRC TCGA cohort (n=508). **(F)** Multivariate cox regression analysis of clinical features and *C3* expression (upper quartile cut-off) in the KIRC TCGA cohort (n=508).

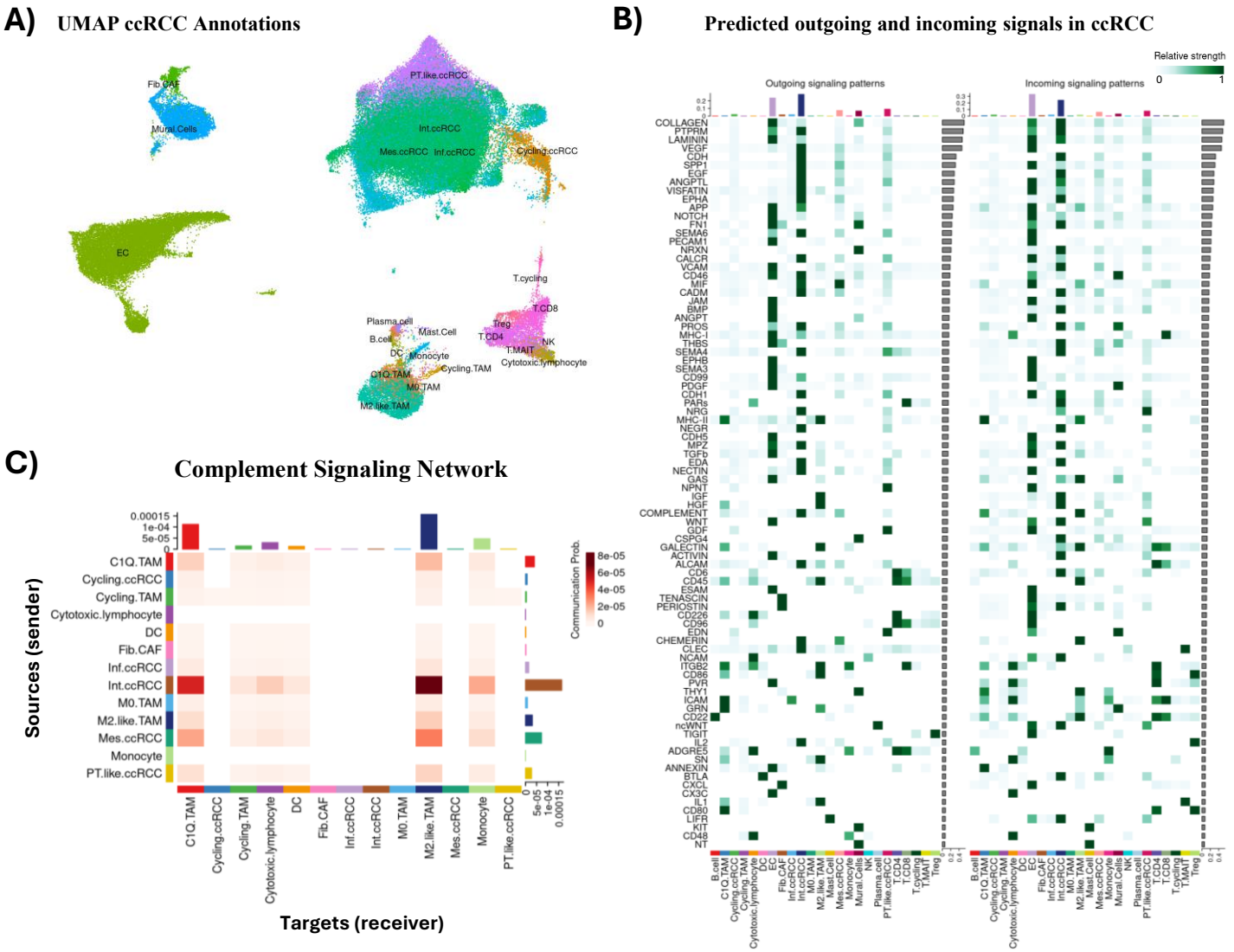

Fig. S5. Global Ligand-Receptor landscape in ccRCC snRNA-seq. (A) UMAP illustrating ccRCC tumor cell annotations employed for ligand-receptor inference (Hu, J., Wang, SG., Hou, Y. et al. 2024, n=20 primary tumors). **(B)** Heatmap of inferred pathway activities by cell group, illustrating relative strength of outgoing (emitting) signaling patterns (left) and incoming (receiving) signaling patterns (right). **(C)** Significant cell to cell communication probabilities inferred for the Complement Signaling Network. Top bars indicate sum of communication probabilities in receiver cells (expressing complement receptors); right bars indicate sum of communication probabilities in emitting cells (expressing complement components).

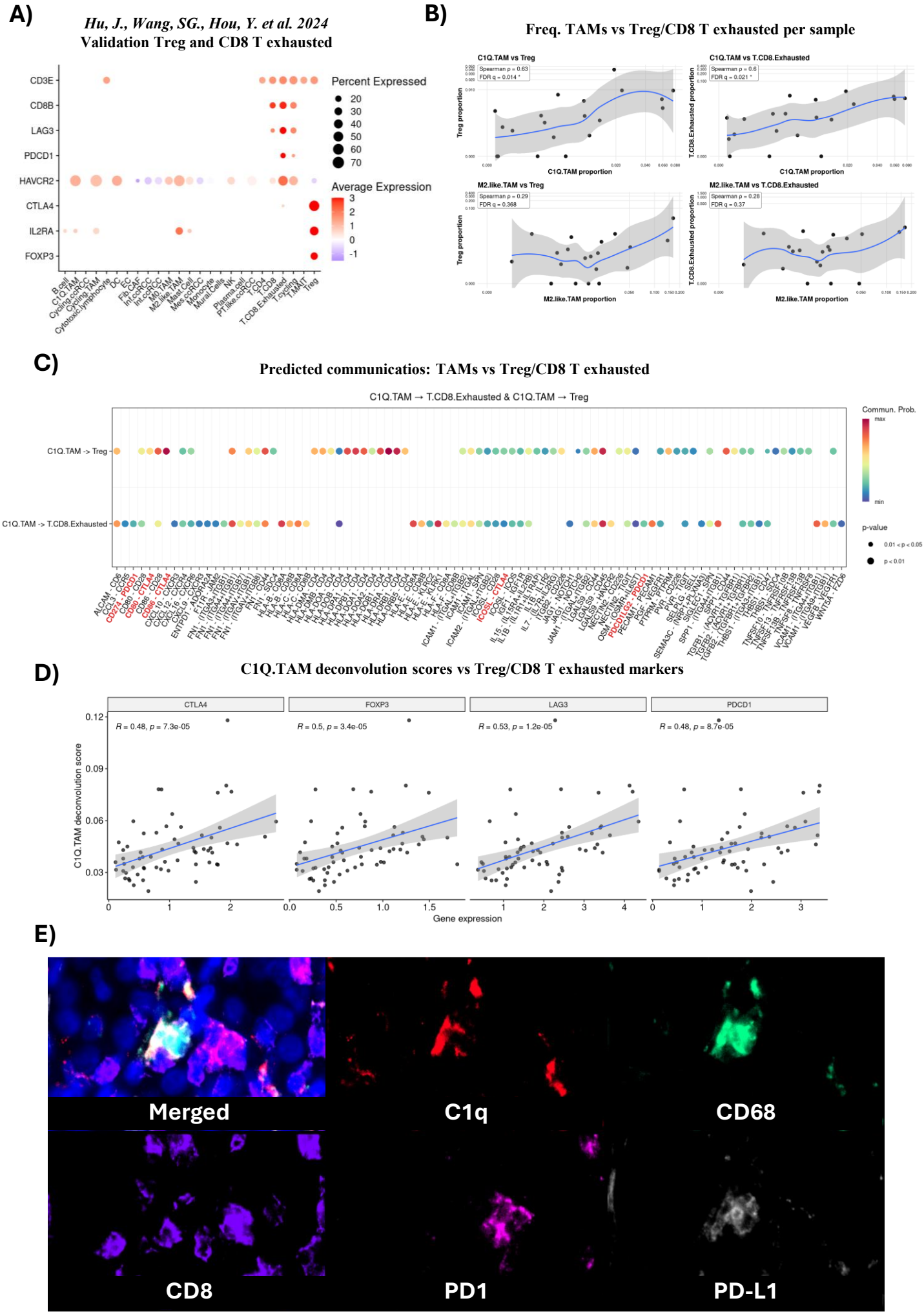

Fig. S6. C1Q-TAMs correlate with Treg and exhausted CD8 T cell abundance in ccRCC.

Fig. S6. C1Q-TAMs correlate with Treg and exhausted CD8 T cell abundance in ccRCC. **(A)** Dot plot displaying key exhausted CD8 T cell and Treg markers, scaled mean expression levels (dot color) and percentage of cells (dot size). **(B)** Scatter plots highlighting correlations between the percetange of TAM cell states (C1Q.TAMs & M2.like.TAMs), exhausted CD8 T cells and Tregs across snRNA-seq tumors (n=20). **(C)** Inferred ligand-receptor pairs sending from C1Q.TAMs to exhausted CD8 T cells or Tregs, immune checkpoint L-R pairs are highlighted in red. Dot color and size represent communication probability, only significant L-R pairs are shown (p.val<0.05). **(D)** Correlation between C1Q.TAM deconvolution scores (CIBERSORTx) and mRNA expression of *CTLA4*, *FOXP3*, *LAG3* and PDCD1 (PD1) in treatment-naïve ccRCC tumors (n=62, (ExhauCRF and ImmPro). **(E)** Representative immunofluorescence image showcasing the close spatial location of C1Q.TAMs and exhausted CD8 T cells; C1q: red; CD68: green; CD8: purple; PD1: pink; PD-L1: white. Nuclei are stained with DAPI.

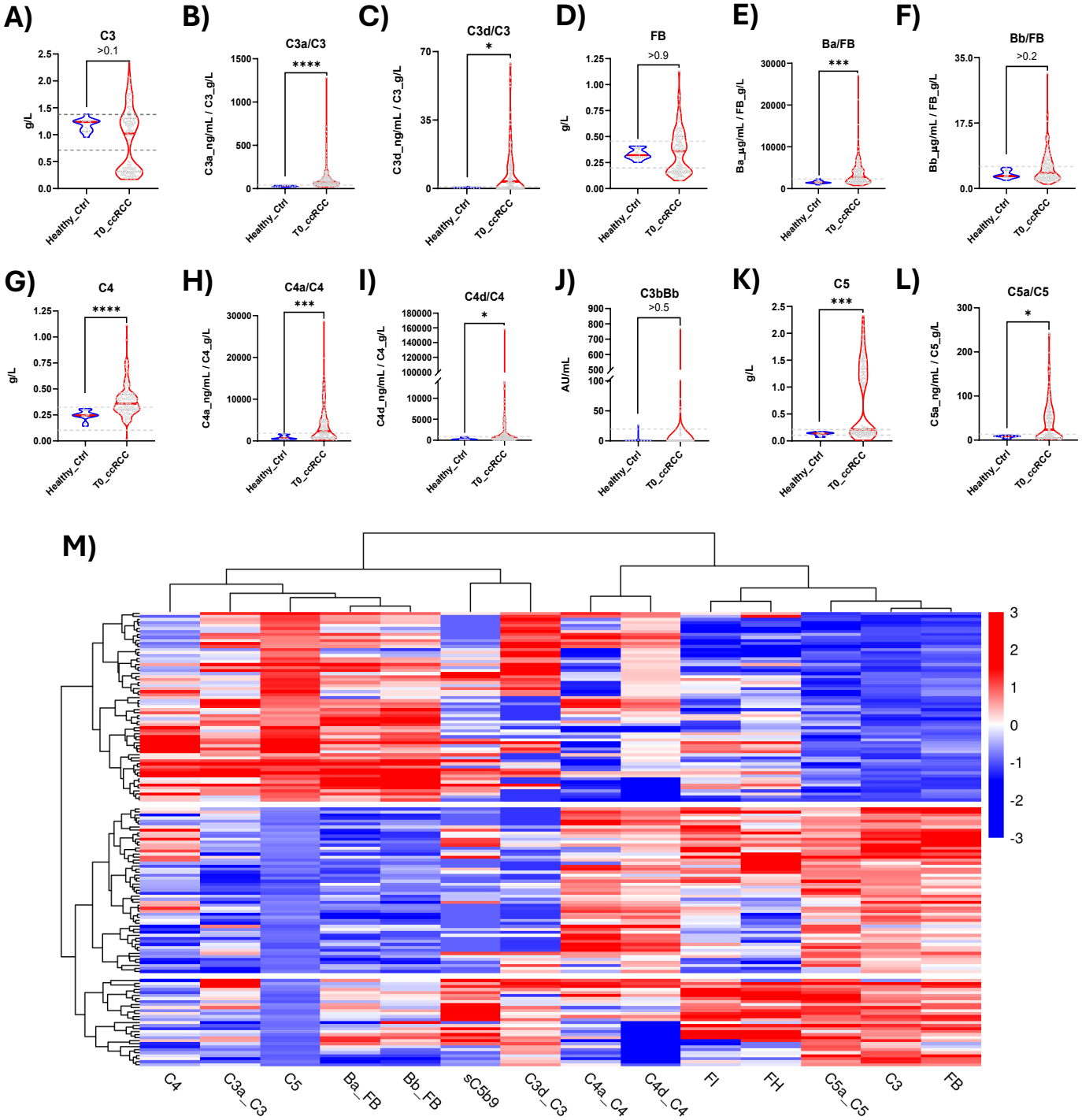

Fig. S7. Complement profiling in metastatic ccRCC patient plasma. (A–L) Comparison of plasma complement components and adjusted activation fragments in metastatic ccRCC patients at baseline (T0, n=147), and in healthy controls (Healthy, n=12). * p-value ≤0,05; ** p-value <0,01, *** p-value <0,001, **** p-value <0,0001. Mann–Whitney test. The cutoff of the normal range is calculated as mean ±2SD or defined by normal healthy ranges in the case of intact complement components. **M)** Heatmap of hierarchically clustered metastatic ccRCC patients (n = 147). Each row represents an individual subject and each column represents a complement feature. Complement measurements are scaled and centred per feature and the range was truncated ±3 SD.

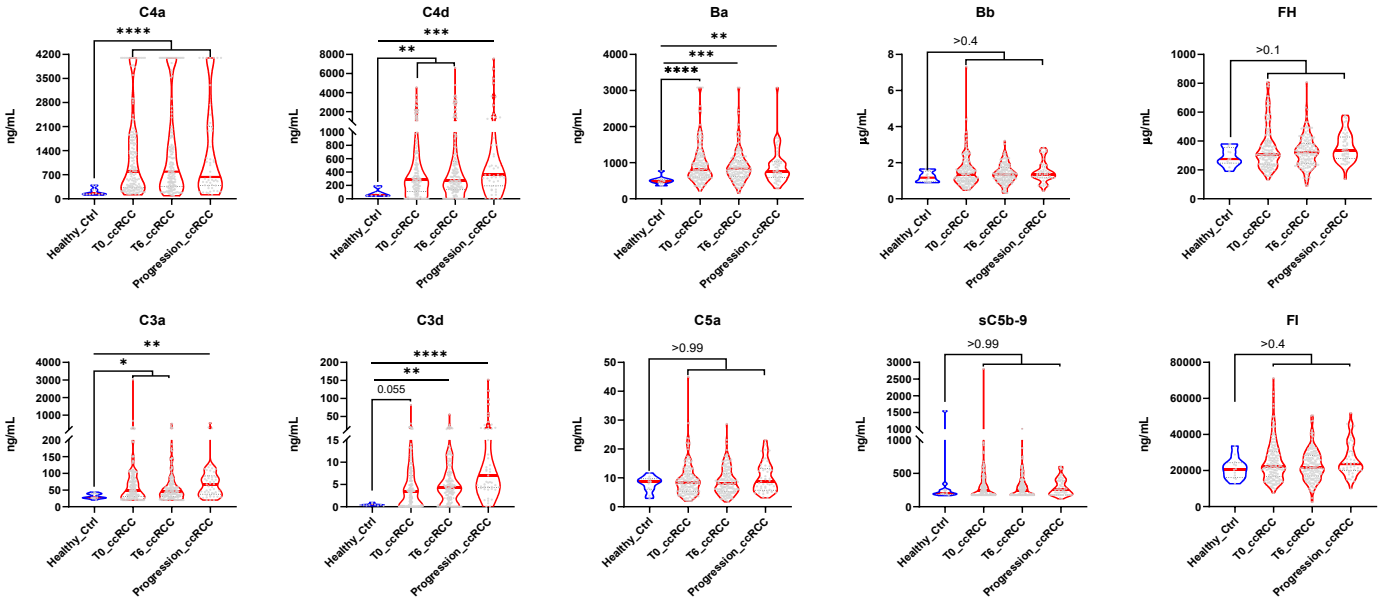

Fig. S8. Complement activation is detectable in plasma across timepoints and treatment arms in metastatic ccRCC. Plasma levels of the indicated complement activation fragments and regulators measured before treatment (T0, n=154), 6 weeks on-treatment (T6, n=153), at progression (Progression, n=49) and in healthy controls (Healthy, n=12). Kruskal Wallis test followed by Dunn's multiple comparisons test was employed using the Healthy control group as reference (*=p.val<0.05, **=p.val<0.01, ***=p.val<0.001, ****=p.val<0.0001).

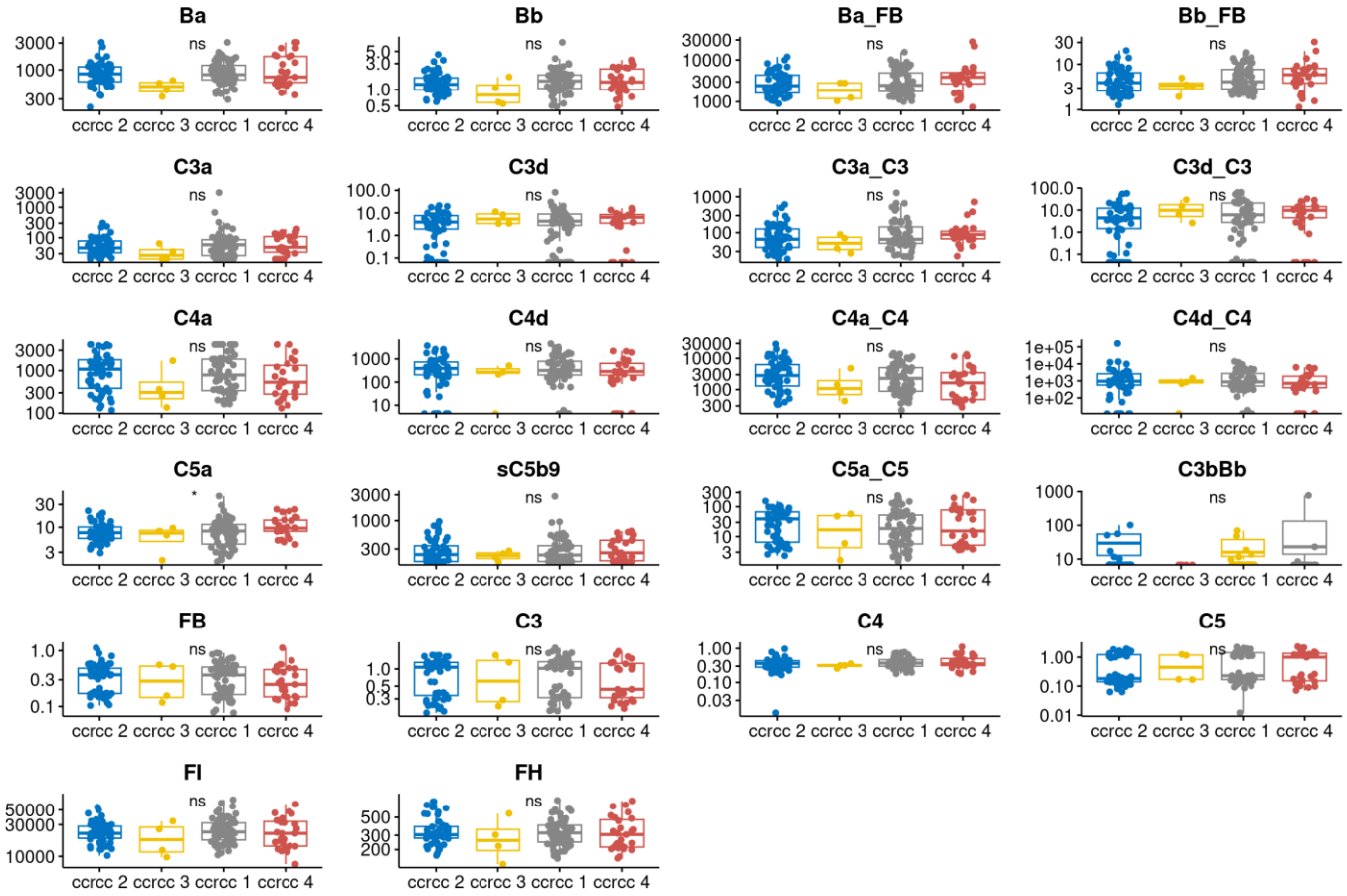

Fig. S9. Plasma complement markers across molecular groups in metastatic ccRCC patient plasma. Comparison of plasma complement components across transcriptomically defined molecular tumour groups: ccrcc1 (n = 83), ccrcc2 (n = 73), ccrcc3 (n = 9), ccrcc4 (n = 34). Kruskal-Wallis test.

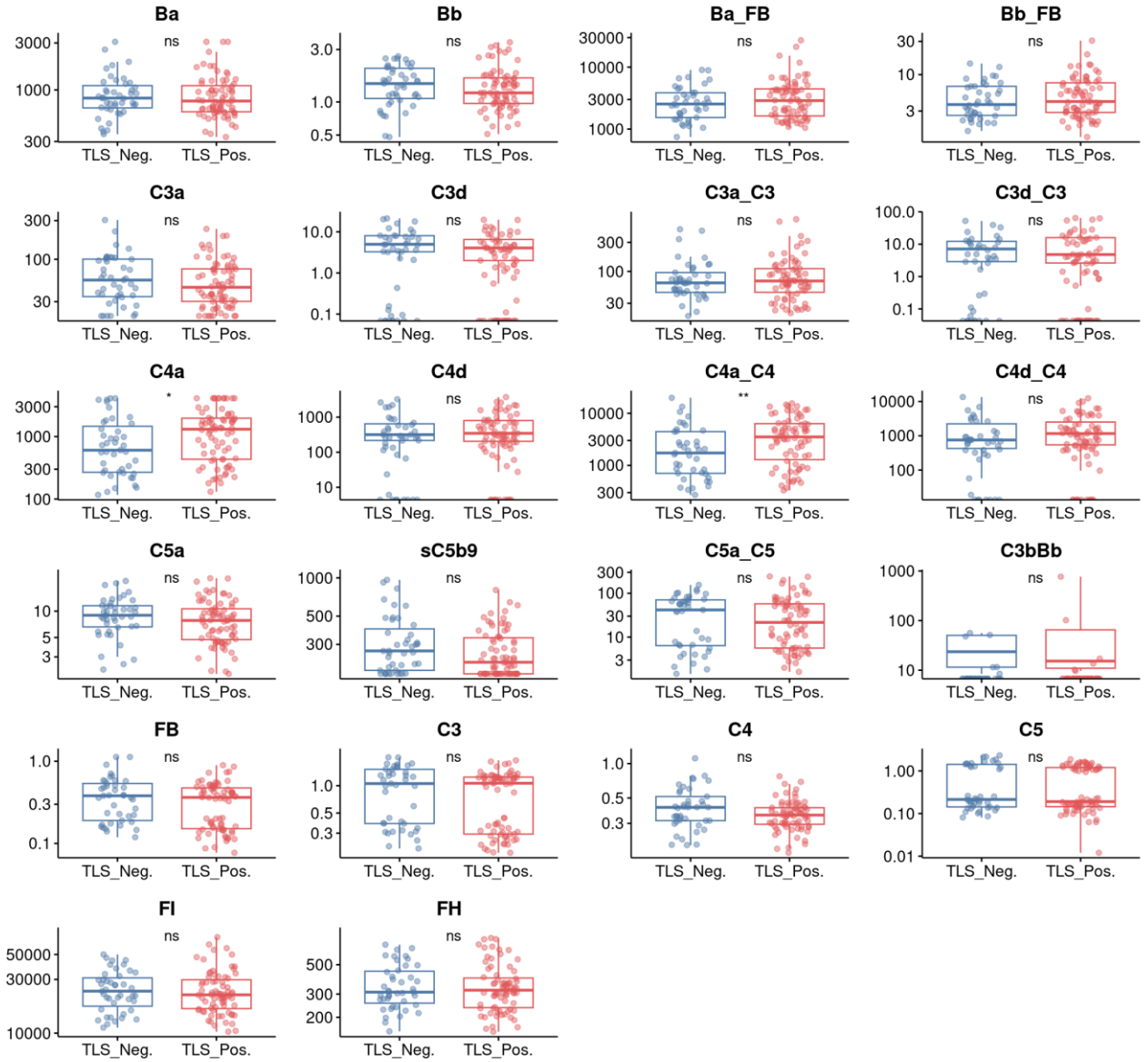

Fig. S10. Plasma complement markers at baseline across TLS positive and negative status. Plasma complement comparisons between patients presenting TLS positive and negative ccRCC tumors. Two-sided Wilcoxon signed-rank test (ns=p.val>0.05, *=p.val<0.05, **=p.val<0.01).

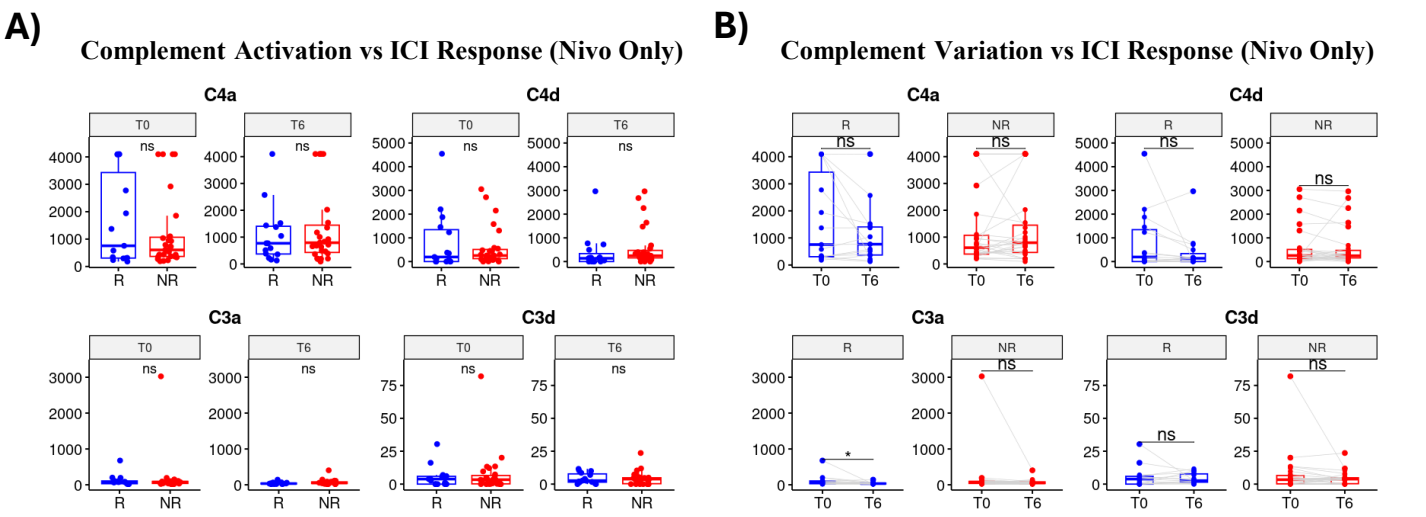

Fig. S11. Complement activation dynamics across response and time in the Nivo treatment arm. (A) Comparisons between R and NR metastatic ccRCC patient plasma before treatment (T0) and 6 weeks on-treatment (T6) in the Nivo arm; two-sided Wilcoxon rank sum test. **(B)** Paired boxplots comparing plasma C4a, C4d, C3a, and C3d levels at baseline (T0) and 6 weeks on-treatment (T6) in responders (R, blue) and non-responders (NR, red) from the Nivo arm. Dots are individual patients and grey lines connect paired samples from the same patient. Within-group T0 vs T6 differences were tested with a paired two-sided Wilcoxon signed-rank test (ns=p.val>0.05, *=p.val<0.05, **=p.val<0.01).

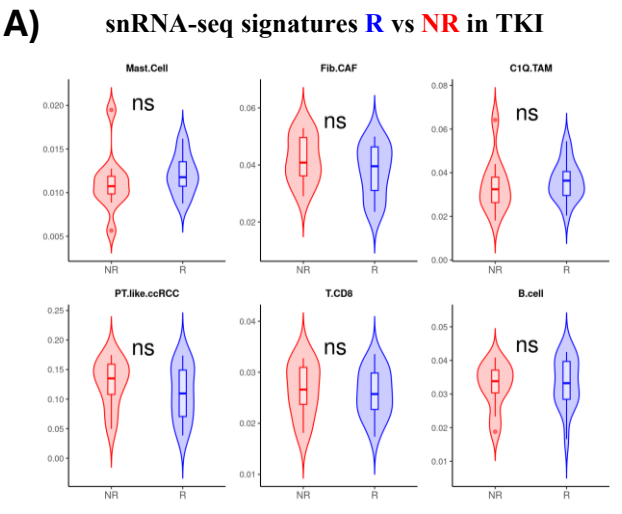

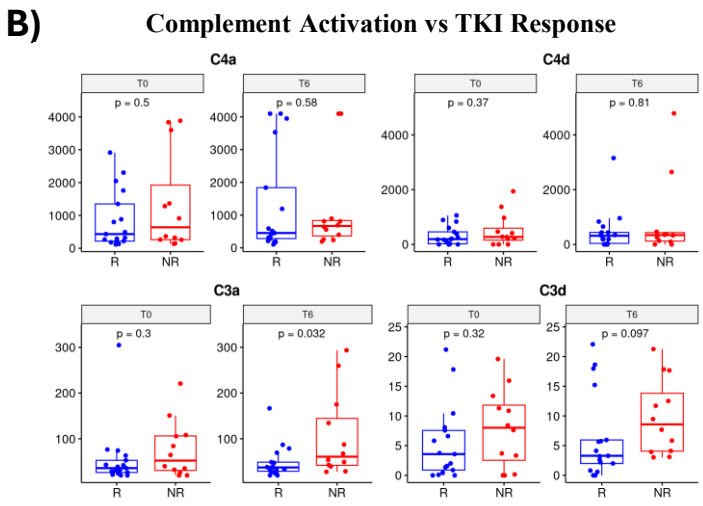

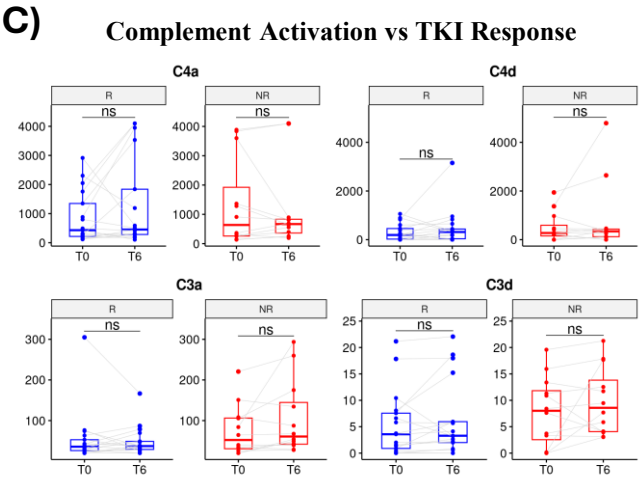

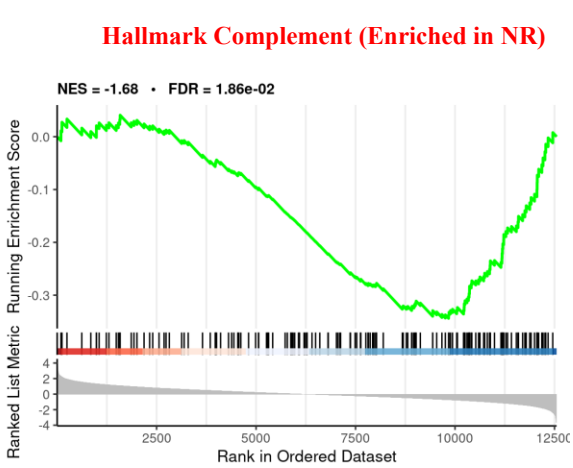

E)

C3a at T6 Mult Logistic Model (NR vs. R)

Response to Nivo-Ipi (NR vs. R)	Odd Ratio (95% C.I.)	*p-value*
C3a at T6 (High C4d)	0.155 (0.018-0.88)	**0.05**
Rhabdoid or Sarcomatoid (Yes)	2.75 (0.36-29.9)	0.35
Number of Metastatic sites (n >1)	0.128 (0.01-0.98)	0.07
IMDC (Good)	0.87 (0.11-6.62)	0.89

Fig. S12. AP activation is linked with worse outcomes in TKI treated patients. (A) Comparison of deconvolution scores in primary tumors for the indicated populations between responders (R, blue) and non responders (NR, red) in the TKI arm (n=25); two-sided Wilcoxon rank sum test (ns = p.val>0.05). **(B)** Comparisons between R and NR metastatic ccRCC patient plasma before treatment (T0) and 6 weeks on-treatment (T6) in TKI arm (n=29); two-sided Wilcoxon rank sum test. **(C)** Paired boxplots comparing plasma C4a, C4d, C3a, and C3d levels at baseline (T0) and 6 weeks on-treatment (T6) in R and NR from the TKI arm. Dots are individual patients and grey lines connect paired samples from the same patient. Within-group T0 vs T6 differences were tested with a paired two-sided Wilcoxon signed-rank test (ns=p.val>0.05, *=p.val<0.05, **=p.val<0.01). **(D)** GSEA plot Complement (Hallmark) highlighting its enrichment in TKI NR. **(E)** Multivariate logistic regression analysis predicting response combining clinical features and C3a levels at T6 (median cut-off) in the TKI arm (n=29, BIONIKK).